Original Article

Evaluation of COC183B2 antibody targeting ovarian cancer by near-infrared fluorescence imaging

Chen Zhang[1,2], Xinyu Ling[3], Yanxiu Guo[1,2], Cunzhong Yuan[4], Hongyan Cheng[1,2], Xue Ye[1,2], Ruiqiong Ma[1,2], Yinli Zhang[5], Yi Li[1], Xiaohong Chang[1,2], Beihua Kong[4], Tao Liu[3], Heng Cui[1,2]

[1]Department of Obstetrics and Gynecology, Peking University People's Hospital, Beijing 100044, China; [2]Center of Gynecologic Oncology, Peking University People's Hospital, Beijing 100044, China; [3]State Key Laboratory of Natural and Biomimetic Drugs, School of Pharmaceutical Sciences, Peking University, Beijing 100191, China; [4]Department of Obstetrics and Gynecology, Qilu Hospital of Shandong University, Jinan 250012, China; [5]Department of Pathology, Peking University People's Hospital, Beijing 100044, China

Correspondence to: Dr. Heng Cui. Department of Obstetrics and Gynecology, Center of Gynecologic Oncology, Peking University People's Hospital, Beijing 100044, China. Email: cuiheng@pkuph.edu.cn.

Abstract

Objective: To evaluate the imaging potential of a novel near-infrared (NIR) probe conjugated to COC183B2 monoclonal antibodies (MAb) in ovarian cancer (OC).

Methods: The expression of OC183B2 antigen in OC was determined by immunohistochemical (IHC) staining using tissue microarrays with the H-score system and immunofluorescence (IF) staining of tumor cell lines. Imaging probes with the NIR fluorescent dye cyanine 7 (Cy7) conjugated to COC183B2 Mab were chemically engineered. OC183B2-positive human OC cells (SKOV3-Luc) were injected subcutaneously into BALB/c nude mice. Bioluminescent imaging (BLI) was performed to detect tumor location and growth. COC183B2-Cy7 at 1.1, 3.3, 10, or 30 μg were used for *in vivo* fluorescence imaging, and phosphate-buffered saline (PBS), free Cy7 dye and mouse isotype immunoglobulin G (IgG)-Cy7 (delivered at the same doses as COC183B2-Cy7) were used as controls.

Results: The expression of OC183B2 with a high H-score was more prevalent in OC tissue than fallopian tube (FT) tissue. Among 417 OC patients, the expression of OC183B2 was significantly correlated with the histological subtype, histological grade, residual tumor size, relapse state and survival status. IF staining demonstrated that COC183B2 specifically expressed in SKOV3 cells but not HeLa cells. *In vivo* NIR fluorescence imaging indicated that COC183B2-Cy7 was mainly distributed in the xenograft and liver with optimal tumor-to-background (T/B) ratios in the xenograft at 30 μg dose. The highest fluorescent signals in the tumor were observed at 96 h post-injection (hpi). *Ex vivo* fluorescence imaging revealed the fluorescent signals mainly from the tumor and liver. IHC analysis confirmed that xenografts were OC183B2 positive.

Conclusions: COC183B2 is a good candidate for NIR fluorescence imaging and imaging-guided surgery in OC.

Keywords: COC183B2 antibody; near-infrared fluorescence imaging; ovarian cancer

Submitted Feb 03, 2019. Accepted for publication Apr 26, 2019.
doi: 10.21147/j.issn.1000-9604.2019.04.11
View this article at: https://doi.org/10.21147/j.issn.1000-9604.2019.04.11

Introduction

Ovarian cancer (OC) is the most lethal gynecologic malignancy. There are an estimated 14,070 OC-related deaths in the United States in 2018, making OC the fifth leading cause of mortality among female cancer patients (1). OC is often diagnosed at late stages because of the lack of obvious and distinctive symptoms. Although the understanding and treatments for OC have developed rapidly in recent decades, the prognosis of advanced-stage

OC patients, especially epithelial tumors, remains far from satisfactory. Recurrence is common, and the overall 5-year survival rate for OC patients is 30%−50%. Cytoreductive surgery combined with chemotherapy is the current mainstream OC treatment. The degree of cytoreduction is one of the most important prognostic factors. However, since surgeons still rely primarily on inaccurate direct visualization methods and empirical tactile feedback to determine tumor margins, optimal cytoreductive surgery results are not achievable, which are defined as minimal residual lesions smaller than 1 cm.

Improved cytoreduction would be possible with a tumor-specific detection strategy, which could contribute to early diagnosis and favorable survival. Traditional imaging techniques, such as X-ray, computed tomography (CT), magnetic resonance imaging (MRI) and ultrasound, have certain limitations due to their nonspecific imaging mechanisms that are mainly based on anatomical changes. Currently, advances in molecular imaging may lead to a new approach of cancer detection and even real-time imaging during operations (2,3). Among the various targeting agents, monoclonal antibodies (MAb) are a well-established class with biological affinity and are probably the most specific imaging probes. The selectivity and high-affinity binding of antibodies to their targets makes antibodies suitable and attractive as image-guided probes upon conjugation with CT contrast agents, paramagnetic particles, radioisotopes or fluorophores (3).

Near-infrared (NIR) fluorescence imaging is an optical imaging in which cells are labeled with proteins or dyes, which have become a preferred method because of its high sensitivity, specificity and low cost. NIR fluorescent probes, such as methylene blue (MB), indocyanine green (ICG), fluorescein (FITC), 5-aminolevulinic acid (5-ALA), IRDye700/800 and cyanine 5/7 (Cy5/7) dyes, are well tolerated in humans and have been widely used in the clinical setting. To date, ICG has been extensively used in cancer surgery for intraoperative sentinel lymph node (SLN) detection in several cancers, such as breast cancer (4), endometrial cancer (5) and gastric cancer (6). However, ICG exhibits dramatic instability *in vivo* with a short plasmatic half-life (2−4 min) and unfavorable self-quenching; most importantly, ICG also binds to plasma proteins with no specificity (7). The NIR fluorescent Cy dyes (650−900 nm), including Cy7 (maximum excitation, 750 nm; maximum emission, 773 nm), are good agents for *in vivo* imaging because of their low nonspecific binding, reduced autofluorescence and increased tissue penetration (8). Wang *et al*. developed a novel bispecific molecular probe named Gd-Cy7-RTP/RGD to target plectin/integrin for MRI/NIR dual-modality imaging and successfully delineate surgical margins during operations for pancreatic cancer (9). Obinutuzumab is the first fully humanized MAb targeting CD20 antigen, labeled with Cy7, and proved to be a promising diagnostic molecular probe for tracking CD20 overexpression in non-Hodgkin's lymphoma (10).

Our previous work used hybridoma technology to generate a high-affinity mouse MAb, COC183B2, which specifically binds to the OC-associated antigen OC183B2 (11,12). Our recent study revealed that ^{131}I-COC183B2 can be used for localizing OC by radioimmunoimaging (13). We later conjugated ultra-small superparamagnetic iron oxide nanoparticles (USPIOs) with the COC183B2 antibody, and this conjugate was used as OC183B2-targeted MRI reagent for early detection of OC (14). However, antibodies labeled with the ^{131}I radionuclide or USPIOs might be toxic. This study evaluated the specificity of COC183B2 antibody in OC using immunohistochemical (IHC) and immunofluorescence (IF) staining and investigated the feasibility of using COC183B2-Cy7 as an *in vivo* NIR fluorescent imaging probe.

Materials and methods

Cells and animals

The murine hybridoma cell line 183B2 and the HeLa cancer cell line preserved in Center of Gynecologic Oncology, Peking University People's Hospital were respectively cultured in 1640 medium supplemented with 15% fetal bovine serum (FBS, Siji Qing, Hangzhou, China) and 1% penicillin/streptomycin (PS, Solarbio, Beijing, China) and DMEM medium supplemented with 10% FBS and 1% PS. The human OC cell line SKOV3-Luc expressing the firefly luciferase gene was kindly provided by Professor Xipeng Wang from Shanghai Jiao Tong University, which was cultured in 1640 medium supplemented with 10% FBS and 1% PS. Cell culture media and supplements were purchased from Life Technologies (Waltham, MA, USA) unless otherwise specified. The animals used in this study were purchased from Beijing Vital River Laboratory Animal Technology Co., Ltd. and housed under specific pathogen-free conditions in the Peking University People's Hospital

Animal Center, with a balanced diet and clean water provided ad libitum. The animals were quarantined for at least 1 week before experiments. This study was approved by the Medical Ethics Committee of Peking University People's Hospital (No. 2016PHC078).

Generation and purification of COC183B2

To generate MAb COC183B2, pristane-pretreated 8-week-old female BALB/c mice were injected intraperitoneally with 5×10^6 hybridoma cells suspended in 200 μL of sterilized phosphate-buffered saline (PBS). After 7 to 10 d, ascites was collected and applied to a protein A affinity chromatography column (Sino Biological Inc., Beijing, China). The purification of COC183B2 was confirmed using 7.5% nonreduced and 13% reduced sodium dodecyl sulfate polyacrylamide gel electrophoresis (SDS-PAGE).

Antigen reactivities of immunized mouse ascites and COC183B2 antibody

The antigen-binding affinities of immunized mouse ascites and MAb COC183B2 were determined by indirect enzyme-linked immunosorbent assay (ELISA). An OC-associated antigen, OC183B2 (2 μg/mL per well), was used to coat a microtitration plate overnight at 4 °C in 0.1 mol/L sodium bicarbonate (pH=9.6). To reduce nonspecific adsorption, the plates were blocked for 1 h at 37 °C with 10% goat serum. The wells were then incubated with 100 μL of different concentrations of ascites (1:8,000, 1:16,000, 1:32,000, 1:64,000, 1:128,000, 1:256,000, and 1:512,000) and antibody (100, 50, 25, 12.5, 6.25, 3.125, 1.563, and 0.781 ng/mL) for 1 h at 37 °C. The same concentrations of a mouse immunoglobulin G (IgG) isotype were used as the negative control. Afterwards, the plates were incubated with horseradish peroxidase (HRP)-labeled goat anti-mouse IgG antibodies (ZSGB-BIO, Beijing, China) for 1 h at 37 °C and then exposed to o-phenylenediamine dihydrochloride/H_2O_2 in a substrate buffer. Fifty microliters of 2 mol/L H_2SO_4 was used to terminate the reaction, and the absorbance at 490 nm was measured with a microplate reader (Tecan Infinite M200, Grödig, Austria).

Tissue microarray (TMA) and immunohistochemistry performed with COC183B2

TMAs with duplicate cores were constructed from 417 OC and 113 fallopian tube (FT) tissue samples collected at Qilu Hospital of Shandong University, between January 2005 and August 2016. The FT tissue samples were harvested from patients who underwent a total hysterectomy and bilateral salpingo-oophorectomy for benign gynecological conditions. IHC staining was performed as previously described (15).

TMA slides were incubated at 65 °C for 1 h, deparaffinized in xylene and rehydrated in a graded ethanol series. To block endogenous peroxidase activity, the slides were treated with Endogenous Enzyme Block (ZSGB-BIO, Beijing, China) for 15 min at room temperature (RT). Antigen retrieval was performed using a microwave oven with citrate buffer (pH=6.0) for 15 min. The TMA slides were then treated with 5% goat serum (ZSGB-BIO, Beijing, China) for 60 min at 37 °C to block nonspecific binding. The primary MAb COC183B2 (10 μg/mL) was incubated on the slides at 4 °C overnight in a humidified chamber, and antibody diluent without the primary antibody was used as a negative control. The next day, the slides were incubated with a goat anti-mouse secondary antibody (ZSGB-BIO, Beijing, China) for 30 min at 37 °C. Finally, the slides were stained with 3,3'-diaminobenzidine (DAB) and hematoxylin for nuclear staining.

Evaluation of IHC staining

The percentage of immunostained cells and staining intensity (0, negative; 1, weak; 2, moderate; and 3, strong) were recorded. The immunointensity of tumor cells was semiquantitatively assessed by using H-score system (16,17). The formula for H-score is as follows: H-score = (percentage of cells with weak intensity staining ×1) + (percentage of cells with moderate intensity staining ×2) + (percentage of cells with strong intensity staining ×3). The scoring was automatically measured by the DensitoQuant module of Quant Center software (3DHISTECH Ltd., Budapest, Öv u. 3., Hungary), and the H-score ranges from 0 to 300. The scores of duplicate specimens were averaged.

IF staining with COC183B2

Cancer cells including SKOV3-Luc and HeLa cells (negative control) were trypsinized and collected. Then, 100 μL of cell suspension was added to 2 μL of antigen retrieval solution (Cytelligen, Taizhou, China), and the mixture was incubated for 10 min at RT. The concentration of Alexa Fluor 488-COC183B2 conjugates (Cytelligen, Taizhou, China) was adjusted to 15 μg/μL in

200 μL of antibody diluent (Cytelligen, Taizhou, China). Then, the cells were incubated with the antibody working solution at RT protected from light for 20 min. The cells used as blank controls received only antibody diluent without the primary antibody. After washing, the cells were mounted with mounting media containing 4',6-diamidino-2-phenylindole (DAPI, Vector Laboratories) for nuclear staining and subjected to automated image scanning and analyses (MetaSystems, Carl Zeiss, Thueringen, Germany).

Antibody labeling with Cy7 and characterization

Conjugation of Cy7 dye with COC183B2 or a mouse isotype IgG antibody was performed according to the manufacturers' instructions. Briefly, 1 mg of Cy7 N-hydroxysuccinimide (NHS) ester (Lumiprobe, Hunt Valley, MD, USA) was dissolved in 147 μL of dimethyl sulfoxide (DMSO) and added to an antibody solution to keep the final concentration of DMSO below 5%. Antibodies (1 mg, 2.8 μmol/L) were incubated with Cy7 NHS ester (56 μmol/L) (mole ratio=1:20) in boric acid/NaOH (pH: 8.3−8.5) at 4 °C protected from light overnight. The eluted solution contained conjugated products, and excess unbound dye was removed using a Zeba Spin Desalting Column, 0.5 mL, 7K MWCO (Thermo Fisher Scientific, Rockford, IL, USA). The protein concentrations of Cy7-conjugated samples were determined by measuring the absorption at 280 nm with a UV-Vis system (Thermo Fisher Scientific). The Cy7 dye concentration was measured as the absorption at 750 nm with the UV-Vis system to determine the number of fluorophore molecules conjugated to each antibody molecule.

Establishment of a xenograft model and treatment groups

OC xenograft mice were established by subcutaneously injecting a cell suspension (100 μL) containing 5×10^6 SKOV3-Luc cells into the right axilla of female BALB/c nude mice (4−5 weeks old). The mice were continuously monitored for tumor growth and used for future experiments when their tumors reached 100−500 mm^3 in volume. To determine the optimal protein dose for NIR fluorescence imaging, a protein dose escalation study was performed in the xenograft mice. A total of 30 mice used in this study were randomly divided into 10 groups with 3 animals per group, and each group was given one of the following treatments: 1) PBS; 2) free Cy7; 3) 1.1 μg IgG-Cy7; 4) 3.3 μg of IgG-Cy7; 5) 10 μg IgG-Cy7; 6) 30 μg IgG-Cy7; 7) 1.1 μg COC183B2-Cy7; 8) 3.3 μg COC183B2-Cy7; 9) 10 μg COC183B2-Cy7; and 10) 30 μg COC183B2-Cy7. Each mouse was intravenously injected via the tail vein with 100 μL of solution containing the corresponding reagents.

Dynamics and targeting ability of Cy7-conjugated COC183B2 in tumor-bearing mice

For *in vivo* experiments, mice were anesthetized with inhaled 5% isoflurane. Serial dorsal images were obtained using the IVIS Spectrum Imaging System (Xenogen, Alameda, CA, USA) at 4, 24, 48, 96, 144, 192 and 264 h after injection of the corresponding reagents via the tail vein to investigate the distribution and targeting ability of the reagents. Bioluminescent imaging (BLI) was conducted to detect SKOV3-Luc tumor cells. Briefly, 150 mg/kg D-luciferin was intraperitoneally injected, and BLI images were collected 10 min after D-luciferin injection. A NIR camera was used to detect Cy7 fluorescence in tumor nodules and major organs. The tumor-to-background (T/B) ratios were analyzed by region of interest (ROI) function and calculated by dividing the fluorescent signal of the tumor by that of surrounding tissue (18) (n=3 per group).

Histological and IHC verification of tumor implants

The mice were sacrificed 264 h after intravenous tail vein injection. At the time of sacrifice, a necropsy was performed on each mouse, and all tumor nodules were collected, fixed and embedded into paraffin blocks. The nodules were stained with hematoxylin-eosin (H&E) to verify the presence of epithelial OC (EOC) and OC183B2 antigen to confirm the establishment of correct animal model.

Statistical analysis

IBM SPSS Statistics (Version 20.0; IBM Corp., New York, USA) was used for statistical analyses. Data are presented as the $\bar{x}\pm s$ from at least three independent experiments. Normality was tested using the Kolmogorov-Smirnov test. Pearson's Chi-square test was used to evaluate OC183B2 expression in clinical specimens. *In vivo* fluorescence imaging comparisons among multiple groups were assessed using a one-way or two-way (two independent variables) analysis of variance (ANOVA) test. $P<0.05$ was considered significant.

Results

Generation and purification of COC183B2 antibody

The mouse ascites titers reached 1:32,000−1:128,000 after immunization process was completed (*Figure 1A*). Highly concentrated COC183B2 antibody was prepared from qualified mouse ascites, and antigen-binding specificity of COC183B2 antibody was detected by ELISA using OC-associated antigen OC183B2 (*Figure 1B*). COC183B2 antibody was purified by protein A affinity chromatography, and purity and molecular weight of the antibody were determined by SDS-PAGE and BandScan 5.0 software (Informer Technologies, Inc., Copthall, Roseau Valley, Dominica) (*Figure 1C*). A single 216.94 kD band was detected under nonreduced conditions, and the reduced SDS-PAGE analysis showed two bands corresponding to heavy chain (47.50 kD) and light chain (25.73 kD). The purity was estimated to be greater than 97%.

OC183B2 expression patterns

The expression of OC183B2 in human OC and FT tissue samples was determined by IHC staining. COC183B2 staining was predominantly localized in the cytoplasm, and the nuclear staining was not dense but showed granulated loci in the OC tissue (*Figure 2A*). The H-score was used to evaluate the immunointensity of COC183B2 staining in tissue samples (17,18). The optimal cutoff for H-score was determined by receiver-operating characteristic (ROC) curve distribution analysis (17). At a total H-score of 300, the threshold for OC183B2 expression was set at 173.26. According to the individual score, the COC183B2 staining results were classified as OC183B2-low (≤173.26) or OC183B2-high (>173.26). The frequency of OC183B2-high samples of OC specimens was substantially higher than that of FT specimens (61.2% *vs*. 46.9%, P=0.006) (*Table 1*). The blank controls showed no COC183B2 staining (data not shown).

To evaluate the role of OC183B2 in OC, we analyzed the relationships between the expression of OC183B2 and clinicopathological features (*Table 2*). OC183B2 expression in serous OC was higher than that in nonserous OC (63.3% *vs*. 43.2%, P=0.010). In addition, the high H-score of OC183B2 was significantly correlated with well-differentiated histology (Grade 1) (P=0.002), smaller residual tumor (≤1 cm) (P<0.001), absence of relapse (P<0.001) and increased survival (P=0.004). However, there was no differences between groups regarding age, menopausal status, International Federation of Gynecology and Obstetrics (FIGO) stage, lymph node metastasis status, ascites, preoperative cancer antigen 125 (CA125) level or platinum resistance (all P>0.05). IF staining with COC183B2 demonstrated strongly positive signals for OC183B2 in both plasma membrane and cytoplasm of SKOV3 cells and no staining in the negative controls (data not shown) or HeLa cells (*Figure 2B*).

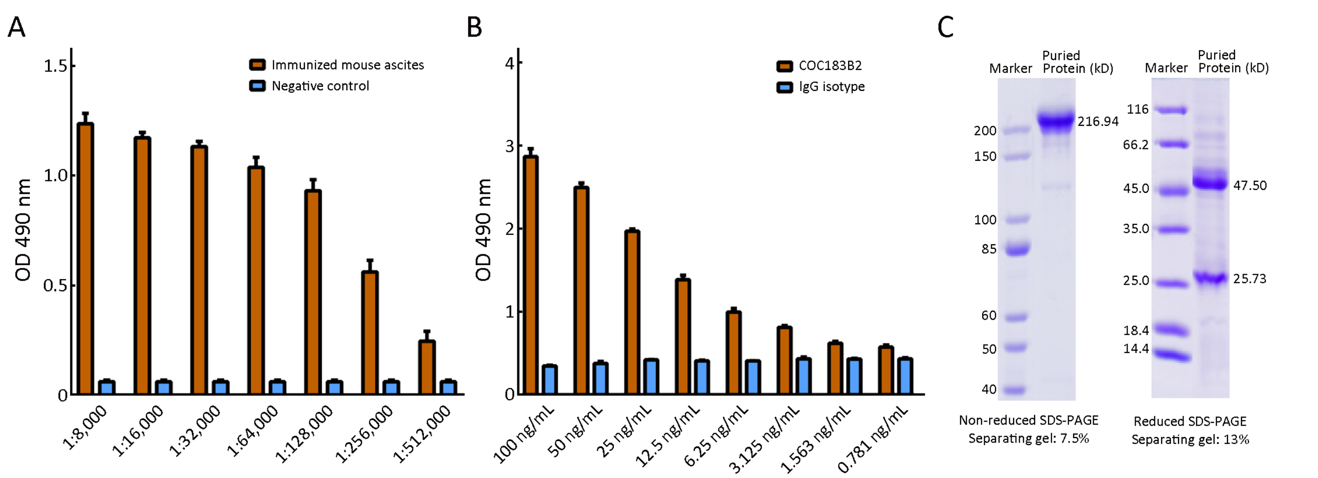

Figure 1 Generation of COC183B2 antibody. (A) Ascites titers for immunized mice reached 1:32,000–1:128,000 after immunization process; (B) Antigen-binding affinity of COC183B2 antibody was determined by enzyme-linked immunosorbent assay (ELISA); (C) Coomassie staining was used to assess the purified COC183B2 antibody under nonreduced and reduced conditions. OD, optical density; SDS-PAGE, sodium dodecyl sulfate polyacrylamide gel electrophoresis.

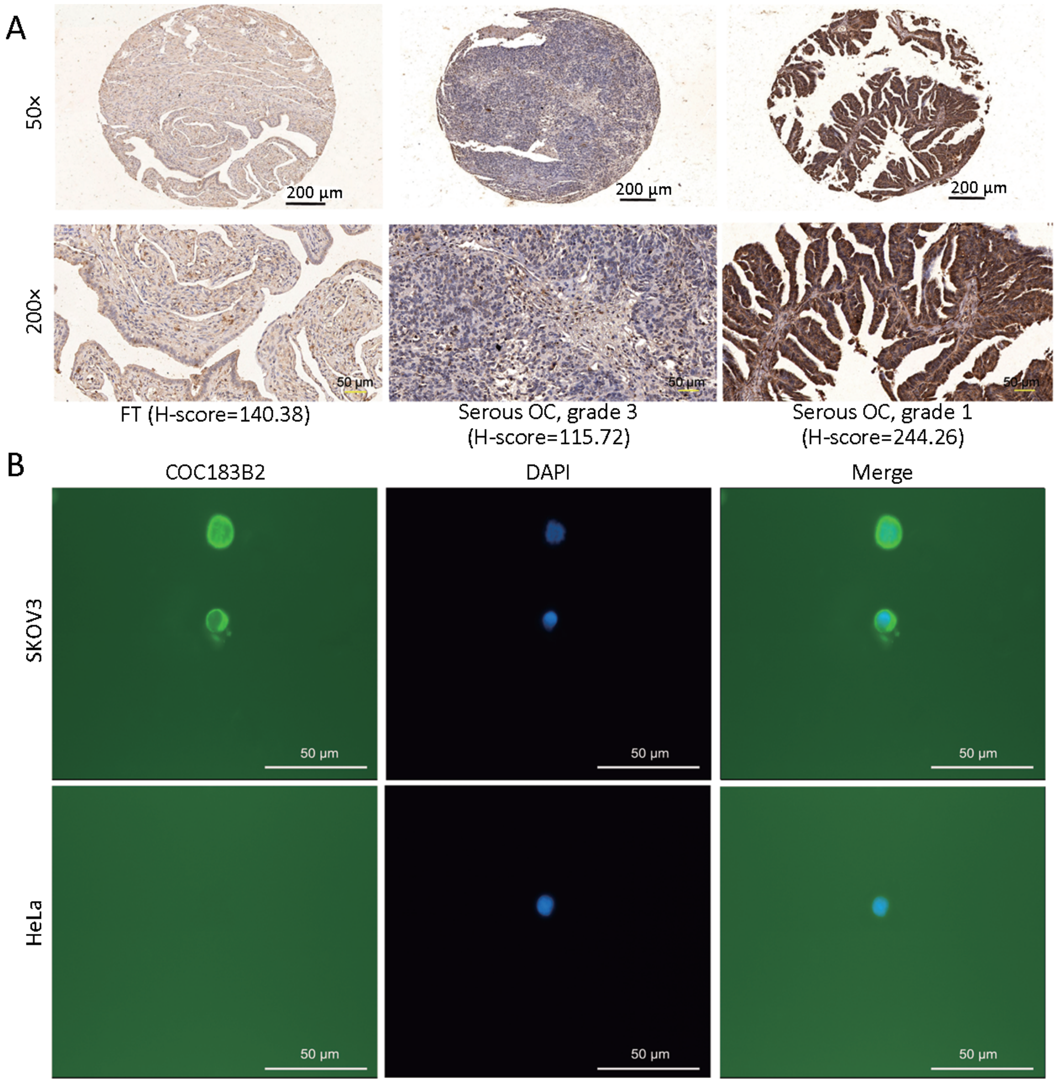

Figure 2 Analyzing specificity of COC183B2 antibody. (A) Representative images of immunohistochemical (IHC) staining with COC183B2 in tissue microarrays (TMAs). Fallopian tube (FT) tissue with a low H-score (140.38); a serous ovarian cancer (OC) tumor (grade 3) with a low H-score (115.72); and a serous OC tumor (grade 1) with a high H-score (244.26). Black scale bar, 200 μm; yellow scale bar, 50 μm; (B) Immunofluorescence (IF) staining of COC183B2 in OC SKOV3 cells and cervical cancer HeLa cells (negative control). COC183B2, green; 4',6-diamidino-2-phenylindole (DAPI), blue. Magnification 400×; white scale bar, 50 μm.

Table 1 OC183B2 expression in all included samples

Group	Samples	OC183B2 expression [n (%)]		χ^2	P
		Low (H-score ≤173.26)	High (H-score >173.26)		
Fimbriae of uterine tube tissues	113	60 (53.1)	53 (46.9)	7.415	0.006
Ovarian cancer tissues	417	162 (38.8)	255 (61.2)		

Synthesis of Cy7 conjugates and in vivo NIR fluorescence imaging

The conjugation and purification processes of Cy7 are summarized in the structure diagram (*Figure 3*). UV-Vis system confirmed that the number of fluorophore molecules per COC183B2 or IgG molecule was about 2–3. The location and growth of SKOV3-Luc tumors were detected by BLI (*Figure 4A*). The results of imaged

Table 2 Association of OC183B2 expression with clinicopathological features of OC patients (417 cases)

Characteristics	n (%)	OC183B2 expression [n (%)]		χ^2	P
		Low (H-score ≤173.26)	High (H-score >173.26)		
Age at diagnosis (year)				1.486	0.223
≤50	149 (35.7)	52 (34.9)	97 (65.1)		
>50	266 (63.8)	109 (41.0)	157 (59.0)		
Unknown	2 (0.5)				
Menopause				0.552	0.458
No	149 (35.7)	56 (37.6)	93 (62.4)		
Yes	254 (60.9)	105 (41.3)	149 (58.7)		
Unknown	14 (3.4)				
Histological subtypes				6.707	0.010
Serous	368 (88.2)	135 (36.7)	233 (63.3)		
Nonserous	44 (10.6)	25 (56.8)	19 (43.2)		
Unknown	5 (1.2)				
FIGO stage				2.702	0.440
I	43 (10.3)	15 (34.9)	28 (65.1)		
II	34 (8.2)	9 (26.5)	25 (73.5)		
III	288 (69.1)	116 (40.3)	172 (59.7)		
IV	18 (4.3)	7 (38.9)	11 (61.1)		
Unknown	34 (8.2)				
Histological grade				12.851	0.002
Grade 1	24 (5.8)	1 (4.2)	23 (95.8)		
Grade 2	17 (4.1)	6 (35.3)	11 (64.7)		
Grade 3	330 (79.1)	135 (40.9)	195 (59.1)		
Unknown	46 (11.0)				
Lymph node metastasis				0.053	0.818
Negative	136 (32.6)	54 (39.7)	82 (60.3)		
Positive	75 (18.0)	31 (41.3)	44 (58.7)		
Unknown	206 (49.4)				
Ascites (mL)				2.450	0.118
<500	86 (20.6)	43 (50.0)	43 (50.0)		
≥500	212 (50.8)	85 (40.1)	127 (59.9)		
Unknown	119 (28.5)				
Preoperative CA125 (U/mL)					
<35	28 (6.7)	7 (25.0)	21 (75.0)	2.666	0.102
≥35	369 (88.5)	150 (40.7)	219 (59.3)		
Unknown	20 (4.8)				
Residual tumor size (cm)					
≤1	136 (32.6)	37 (27.2)	99 (72.8)	13.151	<0.001
>1	59 (14.1)	32 (54.2)	27 (45.8)		
Unknown	222 (53.2)				
Platinum resistance					

Table 2 (*continued*)

Table 2 (*continued*)

Characteristics	n (%)	OC183B2 expression [n (%)]		χ^2	P
		Low (H-score ≤173.26)	High (H-score >173.26)		
No	88 (21.1)	37 (42.0)	51 (58.0)	0.249	0.617
Yes	35 (8.4)	13 (37.1)	22 (62.9)		
Unknown	294 (70.5)				
Relapse					
No	119 (28.5)	29 (24.4)	90 (75.6)	16.584	<0.001
Yes	141 (33.8)	69 (48.9)	72 (51.1)		
Unknown	157 (37.6)				
Death				8.310	0.004
No	176 (42.2)	57 (32.4)	119 (67.6)		
Yes	143 (34.3)	69 (48.3)	74 (51.7)		
Unknown	98 (23.5)				

OC, ovarian cancer; FIGO, International Federation of Gynecology and Obstetrics; CA125, cancer antigen 125.

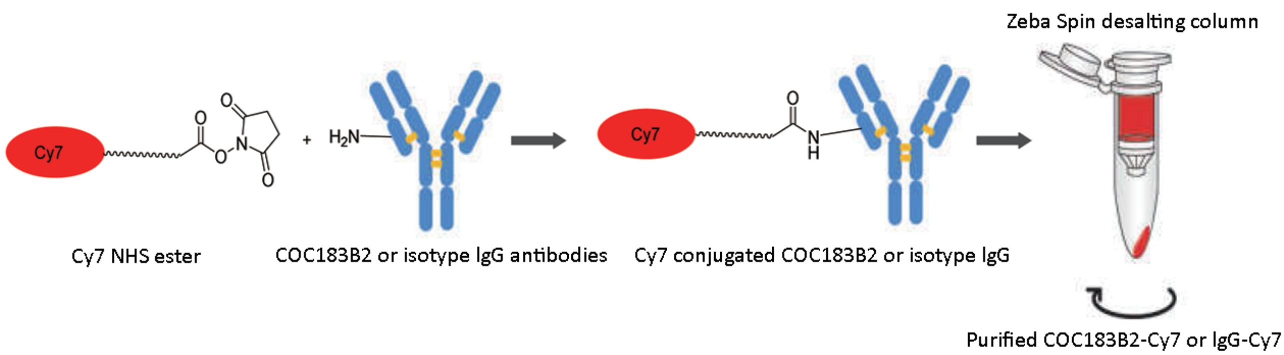

Figure 3 Schematic of conjugation and purification processes of cyanine7 (Cy7) and COC183B2 and mouse isotype immunoglobulin G (IgG) (control) antibodies.

SKOV3-Luc xenograft mice injected with free Cy7 confirmed that the fluorescence observed in the xenograft imaging was not due to Cy7. Cy7 was rapidly distributed throughout the mice, and the dye was cleared and no accumulation was observed at the tumor sites at 24 h post-injection (hpi) (*Figure 4B*). To eliminate the possibility of nonspecific imaging, we also used mouse IgG-Cy7 as a control. We determined the proper dose of COC183B2-Cy7 for *in vivo* NIR fluorescence imaging by comparing the COC183B2-treated groups with the control groups. The T/B ratio of the group receiving 1.1 µg COC183B2-Cy7 was higher than that of PBS group at 4 hpi (P=0.0232) and the corresponding free Cy7 group at 4 hpi (P=0.0012), 24 hpi (P=0.0059) and 144 hpi (P=0.0159) (*Figure 4C*). For the group receiving 3.3 µg COC183B2-Cy7, the T/B ratio was higher than that of PBS group at 4 hpi (P=0.0064) and 24 hpi (P=0.0045) and the corresponding free Cy7 group at 4 hpi (P=0.0003), 24 hpi (P=0.0001) and 144 hpi (P=0.0091), and the 3.3 µg IgG-Cy7 group at 24 hpi (P=0.0002) (*Figure 4D*). Although T/B ratio of 10 µg COC183B2-Cy7 group was significantly higher than that of control groups at nearly all time points (P=0.0043 for IgG-Cy7 *vs*. COC183B2-Cy7 at 264 hpi; P=0.0001 for the other time points), there was no difference between 10 µg IgG-Cy7-treated group and 10 µg COC183B2-Cy7-treated group at 4 hpi (P=0.9521) (*Figure 4E*). The T/B ratio of 30 µg COC183B2-Cy7 group was significantly different compared with control group at all time points (all, P=0.0001) (*Figure 4F*). Moreover, the T/B ratio increased as the protein dose of COC183B2-Cy7 increases. These results indicate that 30 µg COC183B2-Cy7 may be appropriate for *in vivo* NIR fluorescence imaging. The tumor's T/B ratio peaked at 24 h, continued high for 96 h after COC183B2-Cy7 injection, and then gradually

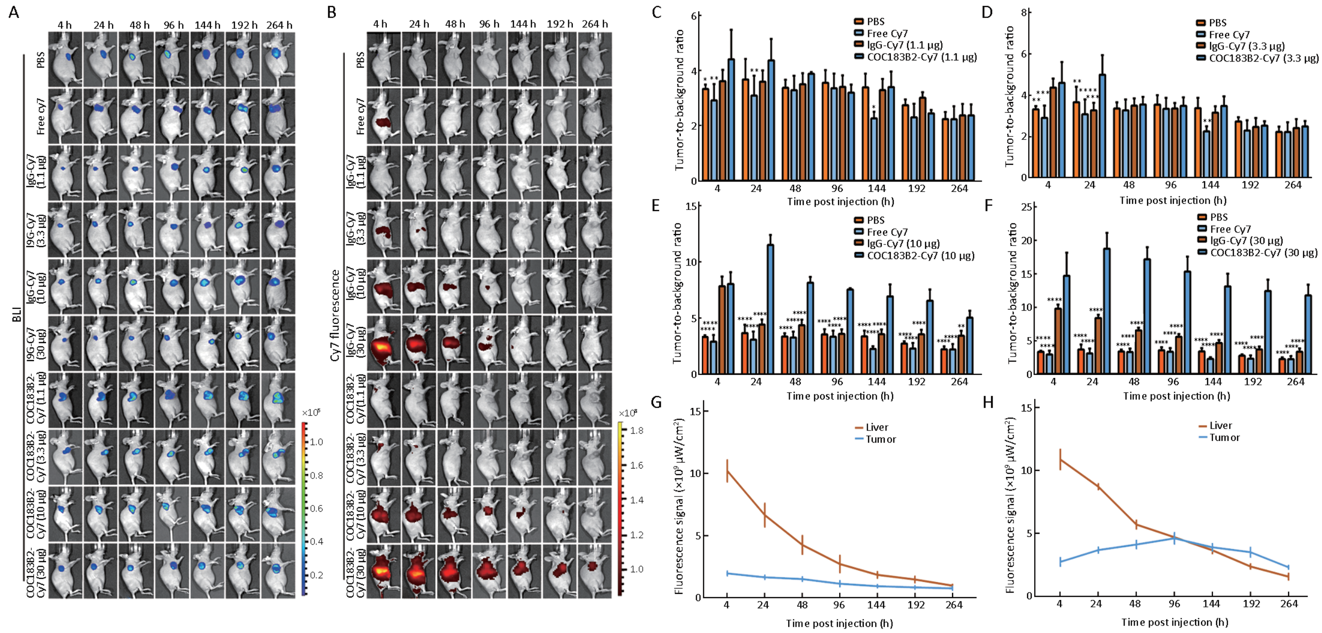

Figure 4 Near-infrared (NIR) imaging of COC183B2-cyanine7 (COC183B2-Cy7) antibody targeting ovarian cancer (OC) tumors *in vivo*. Mice were intravenously injected with phosphate-buffered saline (PBS), free Cy7, or various dose of IgG-Cy7 (n=3 per group). (A) Bioluminescent imaging (BLI) was conducted to detect SKOV3-Luc OC tumor cells at 4, 24, 48, 96, 144, 192, and 264 h post-injection (hpi); (B) NIR imaging of tumor-bearing mice was carried out at the same time points. Tumor-to-background (T/B) ratios of NIR fluorescent signals in tumors are shown for 1.1 μg COC183B2-Cy7 (C), 3.3 μg COC183B2-Cy7 (D), 10 μg COC183B2-Cy7 (E) and 30 μg COC183B2-Cy7 groups (F). T/B ratio of each COC183B2-Cy7 dose group was compared to that of PBS group, free Cy7 group and corresponding IgG-Cy7 dose group at all time points. NIR fluorescent signals of 30 μg IgG-Cy7 (G) and 30 μg COC183B2-Cy7 (H) groups are shown for tumor and liver (n=3). *, P<0.05; **, P<0.01; ***, P<0.001; ****, P<0.0001.

decreased over the next a few days (*Figure 4C−F*). COC183B2-Cy7 was mainly distributed in the xenograft and liver. After intravenous injections of either 30 μg IgG-Cy7 (*Figure 4B,G*) or 30 μg COC183B2-Cy7, Cy7 fluorescence intensity in the liver was high and then decreased. In contrast, Cy7 fluorescence intensity in the tumor of the 30 μg COC183B2-Cy7 group reached the peak level at 96 hpi, while the 30 μg IgG-Cy7 group did not dramatically change at all time points (*Figure 4G,H*). Consequently, COC183B2-Cy7 conjugates specifically aggregated in xenograft tissue. Dorsal images showed a long residence for COC183B2-Cy7 in the xenograft, as tumor accumulation was observed for up to 264 h. During imaging experiments, we did not observe any negative effects on the mice (*i.e.*, weight loss, vomiting or behavioral changes) by administering Cy7 conjugates.

Ex vivo and histological validation of COC183B2 binding

Ex vivo fluorescence images of the tumor and organs at 264 hpi demonstrated that Cy7 fluorescent signals were visible greatly in the tumor and liver, and the signals were also detectable to a lesser extent in the lungs in the 30 μg COC183B2-Cy7 group, while no signals were observed in the other groups (*Figure 5A*). These *ex vivo* images confirmed the *in vivo* analysis (*Figure 4B,H*). H&E staining revealed the formation of epithelial serous OC tumors with features of an irregular cellular shape, a high nuclear-to-cytoplasmic ratio, and a distinct necrotic core (*Figure 5B*). IHC analysis indicated that the xenograft tissue was OC183B2 positive (*Figure 5B*).

Discussion

The identification of specific targets is a necessary step to improve the outcome of OC patients. Our previous study developed MAb COC183B2 and explored the positive staining rate of 75.6% for COC183B2 in epithelial OC tissue (10). In this study, we revealed that the expression of OC183B2 was significantly increased in OC samples compared with FT samples and in serous OC samples compared with nonserous OC samples. In addition, high

OC183B2 levels appear to be significantly associated with clinical characteristics indicating favorable prognosis. Thus, OC183B2 may serve as a potential specific target in OC patients.

The residual tumor size after cytoreductive surgery is one of the most significant prognostic factors in OC and deserves great attention. NIR fluorescence imaging technology with high safety, resolution and sensitivity has emerged as a promising complimentary tool for real-time *in vivo* navigation. Several NIR imaging probes are under investigation at different stages of preclinical research or clinical trials. For example, the imaging of colorectal liver metastasis using ICG might help distinguish patients with malignant liver lesions and benign lesions (18). However, Tummers *et al*. observed no significant difference between the T/B ratios of malignant ovarian lesions and benign ovarian lesions when ICG fluorescence imaging was used in a clinical setting (19). The authors suggest that NIR fluorescence imaging using ICG based on the enhanced permeability and retention (EPR) effect is not suitable for the detection of OC metastasis and requires tumor-specific intraoperative agents.

A promising specific target in epithelial OC is folate receptor alpha (FR-α), which exhibits elevated expression in 90%−95% of patients (20,21). In 2011, the first-in-human intraoperative use of FR-α-targeted agent folate-FITC showed its specificity and sensitivity in OC patients with FR-α-positive tumors (22). However, folate-FITC could not detect malignant tumors that did not express FR-α. Then, NIR fluorescent probes targeting $\alpha_v\beta_3$ integrin (23), Claudin-3 and -4 receptors (24), lysophosphatidic acid (25) and prolactin receptor (26) were investigated for the real-time detection of OC tumors. The overexpression of these targets in OC forms the basis of a new molecular imaging strategy. However, none of these targets is highly expressed in all OC cases, and there is still need to develop specific imaging agents.

In the present study, we used NIR fluorescence imaging

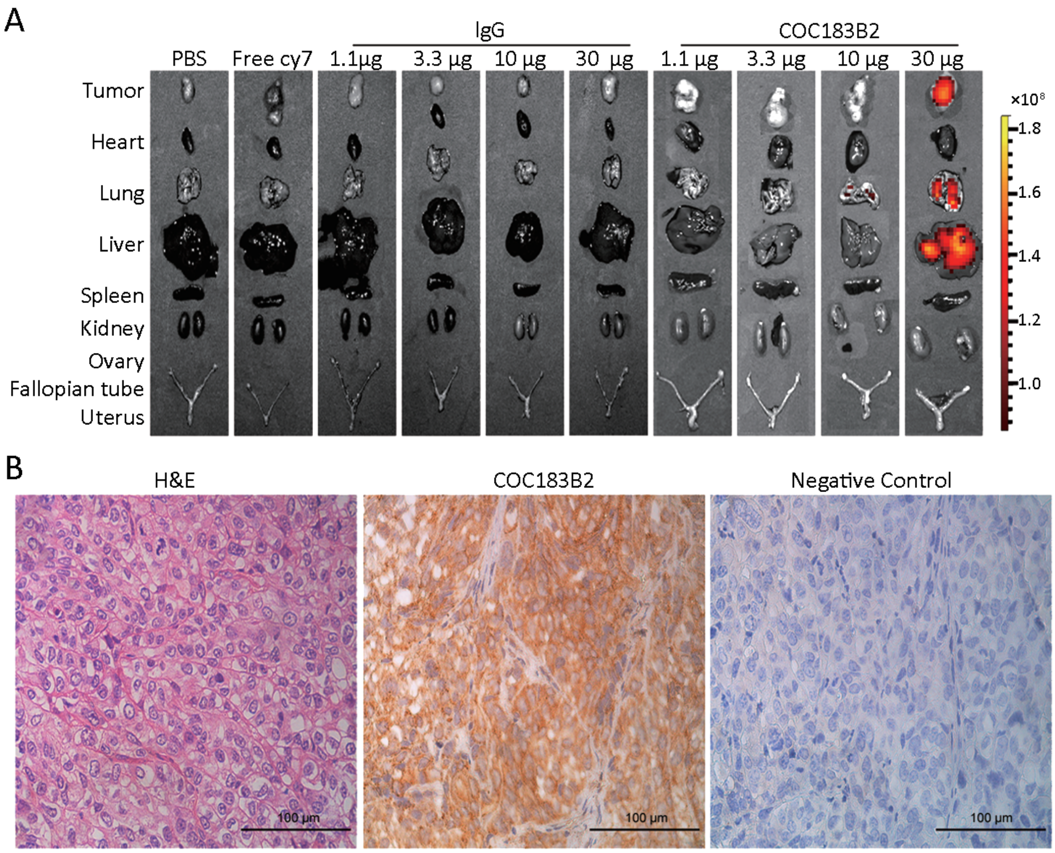

Figure 5 *Ex vivo* and histological validation of COC183B2 binding. (A) Fluorescent signals from the tumor and organs of each group at 264 h post-injection (hpi) were detected; (B) Representative images of resected tumors stained with hematoxylin-eosin (H&E) and immunohistochemistry (IHC) with COC183B2 antibody. Magnification 400×; scale bar, 100 μm. IgG, immunoglobulin G.

to investigate the biodistribution and target efficacy of the antibody COC183B2 labeled with Cy7 fluorophore in the mouse model of serous OC. The mouse model was established using OC cell line SKOV3-Luc expressing luciferase, and assessed with BLI technique, which is a sensitive and reliable method of detecting luciferase activities, anatomical location and *in vivo* progression of tumors without autofluorescence (27). COC183B2-Cy7 specifically accumulated in the xenograft tissue at the ideal dose of 30 μg without noticeable acute or chronic toxicity. Studies (28-30) demonstrated that commercially available epidermal growth factor receptors (EGFR)-specific antibodies labeled with NIR fluorophores can identify head and neck squamous cell carcinoma (HNSCC) with submillimeter resolution during operations (29), and minimal toxicities were observed in the latest phase I trials for panitumumab-IRDye800CW and cetuximab-IRDye800CW (30). Recently, photoimmunotherapy (PIT) has paved the way for precise treatment of cancer by combining conventional photodynamic therapy (PDT) and antibody therapy. Kobayashi and his group developed a novel PIT using on NIR dye-based photosensitizer with MAb targeting EGFR (31), prostate-specific membrane therapy (PSMA) (32) and programmed cell death protein-1 ligand (PD-L1) (33). Target-selective PIT allows the effective targeting based on MAb binding to cell membrane and minimizes side effects. With the efficient targeting of OC and its potential association with a favorable prognosis, the COC183B2 antibody can also be used in the PIT field, which remains to be determined in the future.

Strong tumor signals (a high T/B ratio) are important for reducing false positives and providing useful guidance (34). According to this principle, Heath *et al*. carried out tumor and lymph node resections with real-time fluorescence guidance 48−96 h after the injection of panitumumab-IRDye800CW (28). In this study, the tumor's T/B ratio peaked at 24 h and persisted at 96 h after COC183B2-Cy7 injection. The highest fluorescent signal in the xenografts was detected at 96 hpi, indicating that the possible time window for intraoperative imaging may be 24−96 h after conjugate delivery. *In vivo* imaging and surgery studies in intraperitoneal or orthotopic models are needed to simulate tumor dissemination and metastasis typical of OC to further investigate the optimal temporal window. We observed that liver is the main metabolic organ of COC183B2-Cy7 accumulation, and *ex vivo* fluorescence images at 264 hpi detected fluorescent signals in liver as well as tumor. Compared with smaller molecules such as peptide fragments or nanobodies, antibodies have higher cancer-specific uptake, better bioavailability, longer plasma half-time (days to weeks) and more time to optimally aggregate in tumors (1−2 d) because of their large size (150 kD) (35) that may explain the extended COC183B2-Cy7 residence in the liver. In our future studies, we envisage adapting our methods to relevant antibody fragments, such as antigen-binding fragments (Fabs) and scFvs, to reduce liver retention.

Conclusions

We provide a proof-of-concept study using NIR imaging for cancer detection in an OC model and demonstrate the feasibility and validity of using COC183B2-Cy7 in promising translational applications.

Acknowledgements

This study was supported by the National Key Research and Development Program of China (No. 2016YFA0201400) and National Natural Science Foundation of China (No. 81671431).

Footnote

Conflicts of Interest: The authors have no conflicts of interest to declare.

References

1. Siegel RL, Miller KD, Jemal A. Cancer statistics, 2018. CA Cancer J Clin 2018;68:7-30.
2. Mankoff DA, Farwell MD, Clark AS, et al. Making molecular imaging a clinical tool for precision oncology: A review. JAMA Oncol 2017;3:695-701.
3. Warram JM, de Boer E, Sorace AG, et al. Antibody-based imaging strategies for cancer. Cancer Metastasis Rev 2014;33:809-22.
4. Murawa D, Hirche C, Dresel S, et al. Sentinel lymph node biopsy in breast cancer guided by indocyanine green fluorescence. Br J Surg 2009;96:1289-94.
5. Bodurtha Smith AJ, Fader AN, Tanner EJ, et al. Sentinel lymph node assessment in endometrial cancer: a systematic review and meta-analysis. Am J Obstet Gynecol 2017;216:459-76.e10.
6. Okubo K, Uenosono Y, Arigami T, et al. Quantitative assessment of fluorescence intensity of ICG in

sentinel nodes in early gastric cancer. Gastric Cancer 2018;21:776-81.
7. Porcu EP, Salis A, Gavini E, et al. Indocyanine green delivery systems for tumour detection and treatments. Biotechnol Adv 2016;34:768-89.
8. Kaur S, Venktaraman G, Jain M, et al. Recent trends in antibody-based oncologic imaging. Cancer Lett 2012;315:97-111.
9. Wang Q, Yan H, Jin Y, et al. A novel plectin/integrin-targeted bispecific molecular probe for magnetic resonance/near-infrared imaging of pancreatic cancer. Biomaterials 2018;183:173-84.
10. Lin X, Zhu H, Luo Z, et al. Near-infrared fluorescence imaging of non-Hodgkin's lymphoma CD20 expression using Cy7-conjugated obinutuzumab. Mol Imaging Biol 2014;16:877-87.
11. Qian HN, Feng J, Cui H, et al. Generation and characterization of three monoclonal antibodies to human ovarian epithelial adenocarcinomas. Chin Med J (Engl) 1989;102:839-43.
12. Guo HF, Feng J, Zhang H, et al. Purification and characterization of corresponding antigen recognized by monoclonal antibody 183B2 against ovarian carcinoma. Zhonghua Fu Chan Ke Za Zhi (in Chinese) 2005;40:614-8.
13. Qian HN, Feng J, Cui H, et al. A preliminary study of radioimmunoimaging by 131I-COC183B2 monoclonal antibody in patients with epithelial ovarian cancer. Chin Med J (Engl) 1991;104:109-13.
14. Quan G, Du X, Huo T, et al. Targeted molecular imaging of antigen OC183B2 in ovarian cancers using MR molecular probes. Acad Radiol 2010;17:1468-76.
15. Qian J, Ji F, Ye X, et al. IGHG1 promotes motility likely through epithelial-mesenchymal transition in ovarian cancer. Chin J Cancer Res 2018;30:282-90.
16. Yeo W, Chan SL, Mo FK, et al. Phase I/II study of temsirolimus for patients with unresectable hepatocellular carcinoma (HCC)-a correlative study to explore poteintial biomarkers for response. BMC Cancer 2015;15:395.
17. Azim HA Jr, Peccatori FA, Brohée S, et al. RANK-ligand (RANKL) expression in young breast cancer patients and during pregnancy. Breast Cancer Res 2015;17:24.
18. van der Vorst JR, Schaafsma BE, Hutteman M, et al. Near-infrared fluorescence-guided resection of colorectal liver metastases. Cancer 2013;119:3411-8.
19. Tummers QR, Hoogstins CE, Peters AA, et al. The value of intraoperative near-infrared fluorescence imaging based on enhanced permeability and retention of indocyanine green: feasibility and false-positives in ovarian cancer. PLoS One 2015;10: e0129766.
20. Kalli KR, Oberg AL, Keeney GL, et al. Folate receptor alpha as a tumor target in epithelial ovarian cancer. Gynecol Oncol 2008;108:619-26.
21. Markert S, Lassmann S, Gabriel B, et al. Alpha-folate receptor expression in epithelial ovarian carcinoma and non-neoplastic ovarian tissue. Anticancer Res 2008;28:3567-72.
22. van Dam GM, Themelis G, Crane LM, et al. Intraoperative tumor-specific fluorescence imaging in ovarian cancer by folate receptor-α targeting: first in-human results. Nat Med 2011;17:1315-9.
23. Harlaar NJ, Kelder W, Sarantopoulos A, et al. Real-time near infrared fluorescence (NIRF) intra-operative imaging in ovarian cancer using an $\alpha_v\beta_3$-integrin targeted agent. Gynecol Oncol 2013;128: 590-5.
24. Cocco E, Shapiro EM, Gasparrini S, et al. Clostridium perfringens enterotoxin C-terminal domain labeled to fluorescent dyes for *in vivo* visualization of micrometastatic chemotherapy-resistant ovarian cancer. Int J Cancer 2015;137: 2618-29.
25. Yao D, Lin Z, Wu J. Near-infrared fluorogenic probes with polarity-sensitive emission for *in vivo* imaging of an ovarian cancer biomarker. ACS Appl Mater Interfaces 2016;8:5847-56.
26. Sundaram KM, Zhang Y, Mitra AK, et al. Prolactin receptor-mediated internalization of imaging agents detects epithelial ovarian cancer with enhanced sensitivity and specificity. Cancer Res 2017;77: 1684-96.
27. Vassileva V, Moriyama EH, De Souza R, et al. Efficacy assessment of sustained intraperitoneal paclitaxel therapy in a murine model of ovarian cancer using bioluminescent imaging. Br J Cancer 2008;99:2037-43.
28. Heath CH, Deep NL, Sweeny L, et al. Use of panitumumab-IRDye800 to image microscopic head and neck cancer in an orthotopic surgical model. Ann

Surg Oncol 2012;19:3879-87.
29. Rosenthal EL, Warram JM, de Boer E, et al. Safety and tumor specificity of Cetuximab-IRDye800 for surgical navigation in head and neck cancer. Clin Cancer Res 2015;21:3658-66.
30. Gao RW, Teraphongphom N, de Boer E, et al. Safety of panitumumab-IRDye800CW and centuximab-IRDye800CW for fluorescence-guided surgical navigation in head and neck cancers. Theronostics 2018;8:2488-95.
31. Mitsunaga M, Ogawa M, Kosaka N, et al. Cancer cell-selective *in vivo* near infrared photoimmunotherapy targeting specific membrane mole clues. Nat Med 2011;17:1685-91.
32. Nagaya T, Nakamura Y, Okuyama S, et al. Near-infrared photoimmunotherapy targeting prostate cancer with prostate-specific membrane antigen (PSMA) antibody. Mol Cancer Res 2017;15:1153-62.
33. Nagaya T, Nakamura Y, Sato K, et al. Near infrared photoimmunotherapy with avelumab, an anti-programmed death-ligand 1 (PD-L1) antibody. Oncotarget 2017;8:8807-17.
34. Keereweer S, Sterenborg HJ, Kerrebijn JD, et al. Image-guided surgery in head and neck cancer: current practice and future directions of optical imaging. Head Neck 2012;34:120-6.
35. Kelloff GJ, Krohn KA, Larson SM, et al. The progress and promise of molecular imaging probes in oncologic drug development. Clin Cancer Res 2005;11:7967-85.

Cite this article as: Zhang C, Ling X, Guo Y, Yuan C, Cheng H, Ye X, Ma R, Zhang Y, Li Y, Chang X, Kong B, Liu T, Cui H. Evaluation of COC183B2 antibody targeting ovarian cancer by near-infrared fluorescence imaging. Chin J Cancer Res 2019;31(4):673-685. doi: 10.21147/j.issn.1000-9604.2019.04.11